Structures and energetics of Ga_2O_3 polymorphs

2007 J. Phys.: Condens. Matter 19 346211

(http://iopscience.iop.org/0953-8984/19/34/346211)

IOP PUBLISHING JOURNAL OF PHYSICS: CONDENSED MATTER

J. Phys.: Condens. Matter **19** (2007) 346211 (11pp) doi:10.1088/0953-8984/19/34/346211

Structures and energetics of Ga_2O_3 polymorphs

S Yoshioka, H Hayashi, A Kuwabara, F Oba, K Matsunaga and I Tanaka

Department of Materials Science and Engineering, Kyoto University, Yoshida, Sakyo, Kyoto 606-8501, Japan

Received 16 April 2007, in final form 19 June 2007
Published 20 July 2007
Online at stacks.iop.org/JPhysCM/19/346211

Abstract

First-principles calculations are made for five Ga_2O_3 polymorphs. The structure of ε-Ga_2O_3 with the space group $Pna2_1$ (No. 33, orthorhombic), which is sometimes called κ-Ga_2O_3 in the literature, is consistent with experimental reports. The structure of γ-Ga_2O_3 is optimized within 14 inequivalent configurations of defective spinel structures. Phonon dispersion curves of four polymorphs are obtained. The volume expansivity, bulk modulus, and specific heat at constant volume are computed as a function of temperature within the quasi-harmonic approximation. The Helmholtz free energies of the polymorphs are thus compared. The expansivity shows a relationship of $\beta < \varepsilon < \alpha < \delta$, while $\beta < \varepsilon < \delta < \alpha$ for the bulk modulus. The formation free energies have the tendency $\beta < \varepsilon < \alpha < \delta < \gamma$ at low temperatures. With the increase of temperature, the difference in free energy between the β-phase and the ε-phase becomes smaller. Eventually the ε phase becomes more stable at above 1600 K.

1. Introduction

Gallium oxide (Ga_2O_3) is known to exhibit polymorphism similar to aluminium oxide [1]. In 1952, Roy *et al* reported five polymorphs of Ga_2O_3 [2]. Among them β-Ga_2O_3 with a monoclinic structure was reported to be commonly formed under ordinary conditions. α- and δ-Ga_2O_3 show corundum and bixbyite structures, respectively. γ-Ga_2O_3 is less clearly understood. But it is known to show a spinel structure with some Ga-deficient defects. ε-Ga_2O_3 was found to appear by heating δ-Ga_2O_3 at above 500 °C. Although Roy *et al* reported powder x-ray diffraction intensities, the crystal structure of ε-Ga_2O_3 was not able to be determined. Since then, for more than a half century, little attention has been paid to the structure of ε-Ga_2O_3.

Recently, Sn-doped Ga_2O_3 thin films have been synthesized using the pulsed laser deposition (PLD) technique [3]. The crystal structure found in their study was neither α nor β. It was tentatively assigned as the ε-phase, since their powder x-ray diffraction peaks show some coincidence with those of [2]. The Sn-doped Ga_2O_3 thin film was reinvestigated by the same group recently [4]. They reported that the x-ray diffraction peaks can be identified

using the space group $Pna2_1$ (No. 33, orthorhombic), which is the same as that of the κ-Al_2O_3 phase. However, they also claimed that the phase has higher symmetry than orthorhombic. A first-principles calculation of Ga_2O_3 with the space group $Pna2_1$ was recently reported by Kroll *et al* in the study of the system Ga–O–N [5, 6]. They used κ-Al_2O_3 [7] as the prototype structure and denoted the phase as κ-Ga_2O_3. The lattice parameters and ground-state energies were reported in the work.

In this study, first we investigate the structure of ε-Ga_2O_3 by first-principles calculations. The theoretical results are compared with experimental reports in [2] and [4]. Second, we discuss the atomic arrangement in the defective spinel, γ-Ga_2O_3. Finally the stability of five phases is discussed in terms of the Helmholtz free energy at finite temperatures which is obtained by first-principles lattice dynamics calculations.

2. Computational procedures

The structures of five kinds of Ga_2O_3 polymorph were determined by the projector augmented wave (PAW) [8] method as implemented in the VASP code [9, 10], which is based on the density function theory (DFT) [11]. Plane waves up to an energy cutoff of 360 eV were used as basis functions. The generalized gradient approximation (GGA) as proposed by Perdew, Burke and Ernzerhof was used for exchange and correlation terms [12]. Ga $3d, 4s, 4p$ and O $2s, 2p$ are treated as the valence state. The **k**-point meshes of Brillouin zone sampling for the primitive cells, based on the Monkhorst–Pack scheme [13], were set at $4 \times 4 \times 4$ for α-Ga_2O_3, $5 \times 9 \times 3$ for β-Ga_2O_3, $3 \times 3 \times 3$ for γ-Ga_2O_3, $2 \times 2 \times 2$ for δ-Ga_2O_3, and $2 \times 2 \times 3$ for ε-Ga_2O_3 in order to obtain absolute energy convergence of less than 1 meV/atom. Structural optimization was truncated when the Hellmann–Feynman (HF) forces on all ions became $< 1.0 \times 10^{-3}$ eV Å^{-1}. Regarding γ-Ga_2O_3, there is an ambiguity in atomic arrangement associated with the Ga deficiency. We have constructed 14 different atomic arrangements in 40-atom supercells by $1 \times 1 \times 3$ expansion of the primitive cell of the normal spinel structure. Details will be described later.

Dynamical properties were computed from interatomic force constants in real space through the first-principles calculations [14]. The whole set of force constants was obtained from HF forces generated by a non-equivalent atomic displacement in a supercell for a given crystal structure. In the present study, the dimensions of the supercells were $2 \times 2 \times 2$ the primitive cell for the α structure, and $1 \times 2 \times 2$, $1 \times 2 \times 1$, $1 \times 1 \times 1$ and $2 \times 1 \times 1$ the unit cells for the β, γ, δ and ε structures, respectively. A dynamical matrix was constructed from HF forces acting on all atoms in the supercells with a displaced atom, and phonon frequencies were calculated by solving the eigenvalue problem for the dynamical matrix. In an ionic crystal, displacement of an atom induces a dipole. Dipole–dipole interaction remarkably affects interatomic force constants and causes longitudinal optical/transverse optical (LO/TO) splitting at the wavelength vector $\boldsymbol{k} \approx 0$, namely near the Γ point. Such dipole interaction can be directly included if the size of the supercell is large enough [15]. The non-analytical parameter of Born effective charges [16, 17] also enables one to deal with the LO/TO splitting. The present study does not take into account the influence of dipoles on the interatomic force constant. However, it should be noted that the influence of dipole–dipole interaction is limited to LO modes with the wavelength vector $\boldsymbol{k} \approx 0$, and it leaves the frequencies of TO modes invariant. LO/TO splitting will slightly change the vibrational density of states. This means that the specific heat and other thermodynamical parameters, which are calculated from the vibrational density of states, can be quantitatively discussed without including the LO/TO splitting.

Table 1. Space groups and lattice parameters of Ga_2O_3 polymorphs.

		Lattice parameter	
Phase	Space group	This work	Experiment
α	$R\bar{3}c$	$a = 5.059$ Å	$a = 4.983$ Å[a]
		$c = 13.618$ Å	$c = 13.433$ Å
β	$C2/m$	$a = 12.438$ Å	$a = 12.214$ Å[b]
		$b = 3.084$ Å	$b = 3.037$ Å
		$c = 5.877$ Å	$c = 5.798$ Å
		$\beta = 103.71°$	$\beta = 103.83°$
δ	$Ia3$	$a = 9.401$ Å	$a = 9.52$ Å[c]

[a] Reference [17].
[b] Reference [18].
[c] Reference [20].

3. Results and discussion

3.1. Theoretical structure and band gap of Ga_2O_3 polymorphs

Lattice parameters of Ga_2O_3 polymorphs obtained in the present study are summarized in table 1. Experimental lattice parameters have been well established only for the α- and β-phases. Theoretical values are 1.4 to 1.8% larger than the experimental values [18, 19]. The error is typical for the GGA, which normally overestimates lattice constants by a few per cent. These results are consistent with a previous theoretical report [20]. The lattice parameter of the δ-phase has been less clearly known because the δ-phase is difficult to synthesize without stabilizing elements. Roy *et al* [2] reported that $a = 10.00$ Å, which might be influenced by the presence of water molecules. In their paper, they referred to an older work by Goldschmidt *et al* [21] in which $a = 9.52$ Å was predicted by extrapolation of lattice parameters of In_2O_3–Ga_2O_3 solid solutions. The present result is $a = 9.401$ Å, which is smaller than these experimental values. Taking account of the systematic overestimation for the α- and β-phases, however, the real lattice parameter for the δ-phase may be smaller than the theoretical one ($a \sim 9.3$ Å).

The Kohn–Sham band gaps of α-, β-, δ- and ε-Ga_2O_3 from the present calculations are 2.4, 1.8, 2.3 and 1.9 eV, respectively. For β-Ga_2O_3, the band gap was experimentally reported to be 4.7–4.9 eV [22, 23]. Underestimation by a similar magnitude was reported for β-Ga_2O_3 by a full-potential linearized augmented plane wave calculation within the local density approximation (LDA) [24]. These errors can be ascribed to the GGA or LDA. Analogous results can be seen for ZnO in which the band gap of 3.4 eV [25] has been underestimated to be 0.8–1.0 eV by GGA or LDA calculations [26–28]. Recent theoretical calculations using the B3LYP hybrid functional for the exchange and correlation interactions reported that α- and β-Ga_2O_3 show indirect band gaps of 5.03 and 4.66 eV, respectively, which are much closer to the experimental values [29]. The larger band gap for α- than β-Ga_2O_3 is also found in the present study.

3.2. Structure of ε-Ga_2O_3 phase

The crystal structure of Ga_2O_3 with the space group $Pna2_1$ (No. 33), referred to as the ε-phase or κ-phase, has not been reported so far. It has been considered to have a crystal structure similar to κ-Al_2O_3 in $Pna2_1$ [4]. In order to theoretically investigate the detailed

Table 2. Structural parameters of ε-Ga_2O_3 in the space group $Pna2_1$.

Lattice parameter (Å)		a	b	c		
		5.120	8.792	9.410		
Volume (Å^3)			423.6			
Space group number			33			
Z			8			
Crystal system			Orthorhombic			
Theoretical density (g cm^{-3})			5.88			
Element	Number	Wyckoff position		x	y	z	Occupancy
Ga	1	4a		0.1777	0.1522	0.9980	1
Ga	2	4a		0.8127	0.1617	0.3087	1
Ga	3	4a		0.1911	0.1504	0.5874	1
Ga	4	4a		0.6781	0.0322	0.7960	1
O	1	4a		0.9705	0.3247	0.4259	1
O	2	4a		0.5228	0.4885	0.4331	1
O	3	4a		0.6514	0.0016	0.2043	1
O	4	4a		0.1535	0.1586	0.1975	1
O	5	4a		0.8480	0.1709	0.6705	1
O	6	4a		0.5192	0.1678	0.9383	1

internal position of ε-Ga_2O_3 with the space group, geometry optimization is performed using the structure of κ-Al_2O_3 as an initial input. Table 2 shows the resultant structural parameters of ε-Ga_2O_3. The lattice parameters are $a = 5.120$, $b = 8.792$, and $c = 9.410$ Å, which are 1.6, 0.7 and 1.6% larger than the experimental values reported recently for Sn-doped Ga_2O_3 [4]. The theoretical data by Kroll *et al* for κ-Ga_2O_3 are 5.0566, 8.6873 and 9.3072 Å in [5], which are 1.0–1.2% smaller than the present results. In [6], however, the same authors reported that the theoretical cell volume increased by approximately 2% when Ga d electrons were treated as the valence state.

Table 3 shows the theoretical interplanar spacings and x-ray powder diffraction intensities of ε-Ga_2O_3 by Cu Kα ($\lambda = 1.5406$ Å) radiation. The lattice parameters are isotropically compressed by 2% in order to roughly correct the error. XRD data from the Roy's paper [2] are also shown. The positions of major diffraction peaks such as those at 28.1°, 30.7° and 33.4° agree well with the experimental results [2].

3.3. Structure of γ-Ga_2O_3 phase

For γ-Ga_2O_3, 40-atom supercells with different atomic arrangements were used, which were obtained by expanding the primitive cell of the normal spinel structure by three times only along the c-axis, i.e., $1 \times 1 \times 3$ expansion. Each of them is composed of 6 tetrahedral cationic sites, 12 octahedral cationic sites and 24 oxygen sites. Among the 18 cationic sites, 2 sites were chosen to be vacant. Taking account of symmetry of the defects, we can find 14 different structures. A similar analysis was made on γ-Al_2O_3 in [30] using 40-atom supercells. They also found 14 inequivalent configurations.

Calculations were made for all of 14 inequivalent structures. The results are summarized in figure 1(a), where the relative energy of each structure is plotted against the vacancy–vacancy distance in the geometry before the optimization procedure. Cell volumes are shown in a similar way in figure 1(b). As can be noted, there is no correlation between the vacancy–vacancy distance and relative energy. Also, no correlation can be seen with the cell volume. The energies of the 14 structures are scattered within a range of 0.49 eV per formula unit.

Table 3. Interplanar spacing and Miller's indices for ε-Ga_2O_3.

This study							Experimental[a]		
d	d (−2%)	2θ (−2%)	h	k	l	I/I_0	d	2θ	I/I_0
6.444	6.318	14.01	0	1	1	8	6.42	13.78	4
4.721	4.629	19.16	0	0	2	5	4.67	18.99	4
4.447	4.360	20.35	1	1	0	2			
3.348	3.283	27.14	1	2	0	6			
3.236	3.173	28.10	1	1	2	12	3.17	28.13	26
3.222	3.159	28.22	0	2	2	17			
3.156	3.095	28.83	1	2	1	3			
2.965	2.906	30.74	0	1	3	42	2.926	30.53	50
2.807	2.752	32.51	0	3	1	2			
2.731	2.678	33.43	1	2	2	100	2.693	33.24	100
2.574	2.524	35.54	2	0	0	13	2.528	35.48	40
2.569	2.518	35.62	1	1	3	14			
2.552	2.502	35.86	1	3	0	8			
2.483	2.435	36.89	2	0	1	12	2.434	36.90	60
2.471	2.422	37.08	2	1	0	3			
2.464	2.416	37.19	1	3	1	26			
2.361	2.314	38.88	0	0	4	3	2.328	38.64	64
2.293	2.249	40.07	1	2	3	9	2.22	40.61	10
2.260	2.215	40.69	2	0	2	8			
2.246	2.202	40.96	1	3	2	21			
2.205	2.161	41.76	0	4	0	4			
2.189	2.146	42.06	2	2	1	14			
2.027	1.987	45.62	1	4	0	3			
2.011	1.972	45.99	2	2	2	2			
1.998	1.959	46.32	0	4	2	6	1.96	46.28	12
1.993	1.954	46.44	2	0	3	5			
1.982	1.944	46.70	1	3	3	10			
1.943	1.905	47.69	2	1	3	8	1.91	47.57	4
1.863	1.826	49.90	1	4	2	4	1.83	49.79	4
1.847	1.810	50.36	0	1	5	3			
1.816	1.780	51.28	2	2	3	3			
1.740	1.706	53.69	2	0	4	10	1.706	53.68	24
1.733	1.699	53.92	1	3	4	7			
1.587	1.556	59.37	3	1	2	4	1.55	59.60	64
1.539	1.509	61.41	0	5	3	10			
1.523	1.493	62.13	2	0	5	11	1.494	62.07	48
1.518	1.488	62.33	1	3	5	26	1.452	64.08	40
1.482	1.453	64.03	3	−3	0	23			
1.470	1.441	64.63	0	6	0	10	1.4	66.76	8
1.426	1.398	66.89	3	2	3	8			
1.391	1.363	68.81	2	5	2	5	1.37	68.42	4
1.340	1.313	71.82	0	1	7	3	1.32	71.40	3

[a] Reference [2].

In the lowest-energy structure, two Ga vacancies are located at the octahedral sites. The vacancy–vacancy distance for this model is 8.06 Å. On the other hand, in the second-lowest energy structure, vacancies are located at both tetrahedral and octahedral sites with a vacancy–vacancy distance of 3.57 Å. These results indicate the absence of a clear preference for site occupancies.

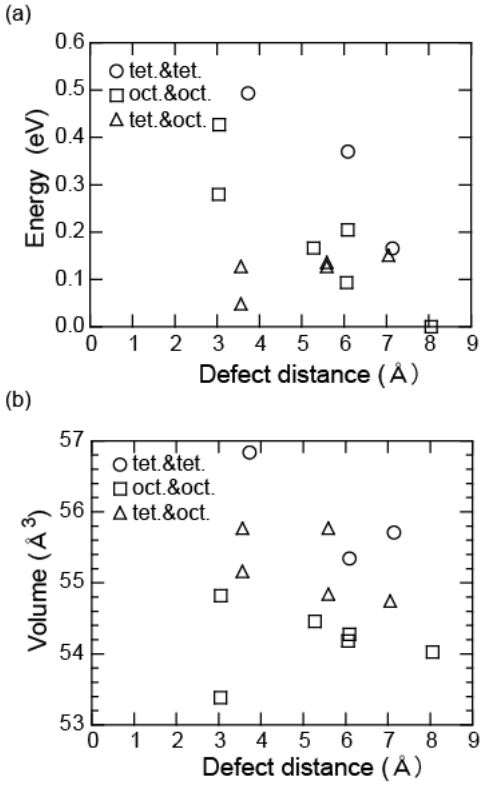

Figure 1. Relative energies (a) and volumes (b) per formula unit of 14 inequivalent structures for γ-Ga_2O_3 against the vacancy–vacancy distance.

3.4. Phonon dispersion and finite temperature properties of Ga_2O_3 polymorphs

Figure 2 shows phonon dispersion curves of the five polymorphs, α, β, γ, δ and ε. For the γ-structure, the one with the lowest energy in figure 1 has been adopted. None of them exhibit imaginary frequency. The density of states (DOS) of the phonon and their partial components per atom are shown together. Since Ga is heavier than O, O makes a greater contribution to high frequencies than Ga in all phases. The phonon DOS is used to discuss the finite-temperature energetics.

Based on the quasi-harmonic approximation (QHA), we can obtain the Helmholtz free energy (F), entropy of vibration (S_{vib}) and specific heat at constant volume (C_V) at finite temperatures from the phonon DOS at various lattice volumes (V) [31]. Because of the uncertainty in the crystal structure, the γ-phase is not subject to further analyses. Figure 3 shows the calculated Helmholtz free energies of the α-, β-, δ- and ε-phases against lattice volume at temperatures from 0 to 1500 K. The lattice volume with minimum free energy is determined by fitting curves to the third-order Birch–Murnaghan equation of states at each temperature under the condition of $\partial B/\partial P = 4$, where B and P are the isothermal bulk modulus and pressure, respectively [32]. Minimum energy points are connected by a dotted curve in figure 3. As shown in this figure, the lattice volume becomes larger with the increase of temperature. The thermal volume expansion can be computed within the QHA in this way. Figure 4(a) shows the volume expansivity with reference to the value at 297 K. The expansivity

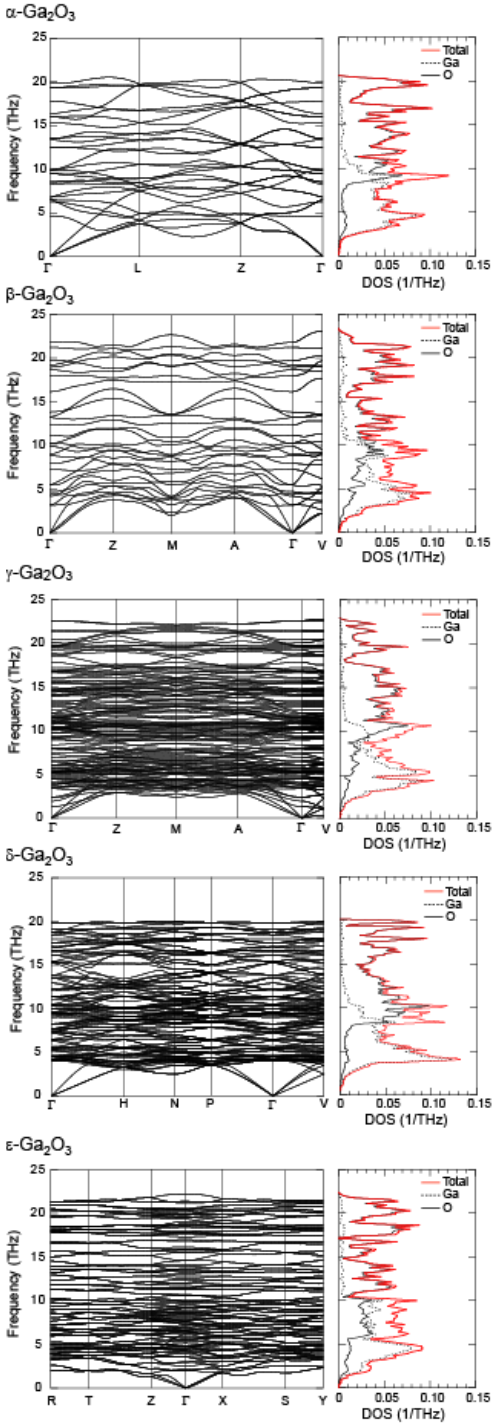

Figure 2. Phonon dispersion curves and DOS for α-, β-, γ-, δ- and ε-Ga_2O_3.
(This figure is in colour only in the electronic version)

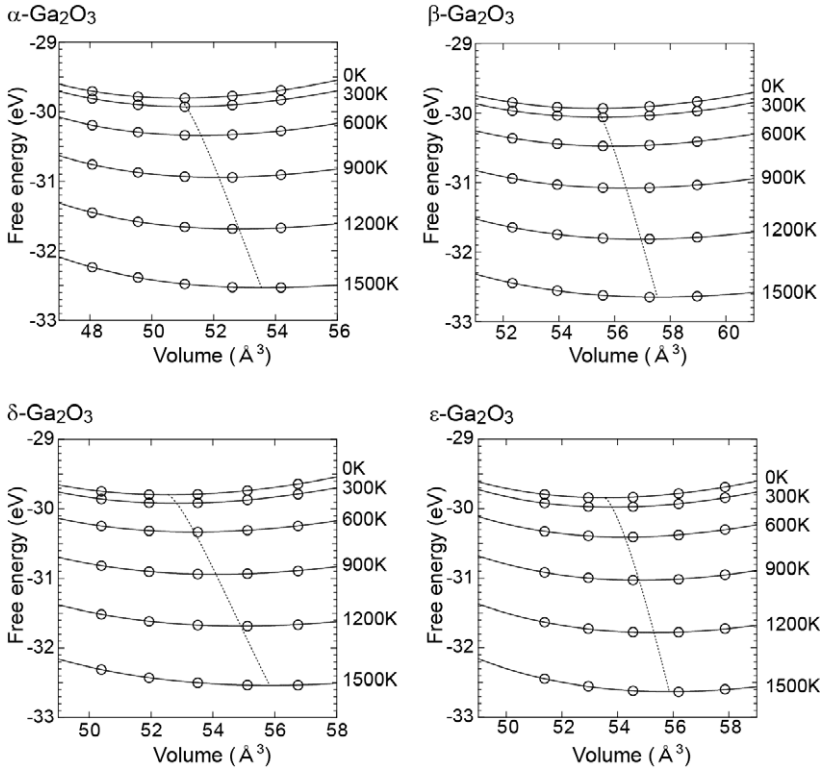

Figure 3. Plots of Helmholtz free energy against lattice volume per formula unit for α-, β-, δ- and ε-Ga_2O_3 from 0 to 1500 K.

is smallest in the β-phase and increases in the order β, ε, α, and δ. The expansivity of the α-phase agrees well with the experimental data [33]. Bulk moduli for the four phases are shown in figure 4(b). As can be noted, the calculated moduli increase in the order β, ε, δ, and α below 400 K.

The experimental specific heat is available only for the β-phase. Figure 5 shows the experimental specific heat at constant pressure, C_p [34, 35], with computed C_V and C_p, where C_V is the specific heat at constant volume. Since the cell volumes are fixed during the present calculations, C_V values can directly be obtained by the lattice dynamics method, while C_p values are evaluated using the thermodynamical relationship $C_p - C_V = \alpha^2 V B T$, where α is the thermal expansivity. As can be seen, the agreement between theory and experiment is quite satisfactory.

Then the Helmholtz free energies were computed as a function of temperature for α-, β-, ε- and δ-phases. The Helmholtz free energy differences of the α-, β-, δ-, ε- and γ-phases are shown in figure 6. From these plots, the relative stability for the five phases can be discussed. According to the present calculation, the β-phase is the most stable phase at temperatures below 1500 K. In the previous section, we found that the lowest-energy γ-phase is 0.19 eV per formula unit higher in energy than the β-phase at 0 K. The formation energies are, therefore, in the sequence $\beta < \varepsilon < \alpha < \delta < \gamma$ at low temperatures. With the increase of temperature, the difference in free energy between the β-phase and the ε-phase, $\Delta F_{\varepsilon-\beta}$, becomes smaller, and vanishes at around 1600 K. The larger temperature dependence of the ε-phase can be ascribed to the larger thermal entropy.

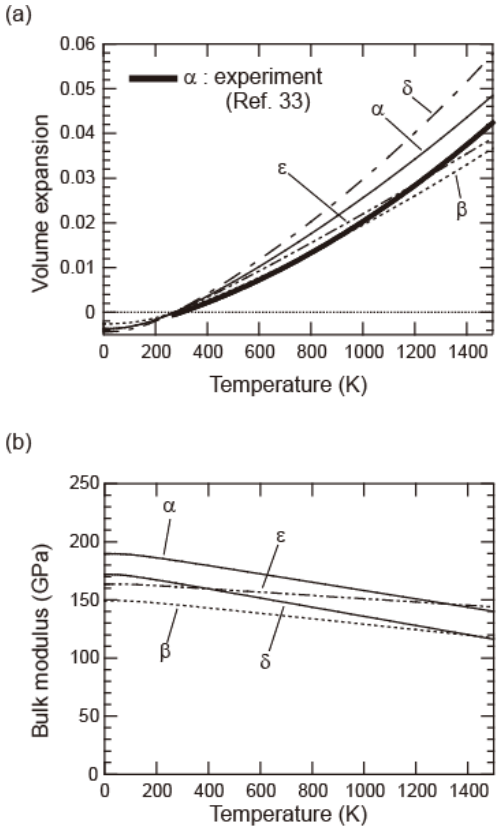

Figure 4. Temperature dependence of volume expansivity (a) and bulk modulus (b) for α-, β-, δ- and ε-Ga_2O_3.

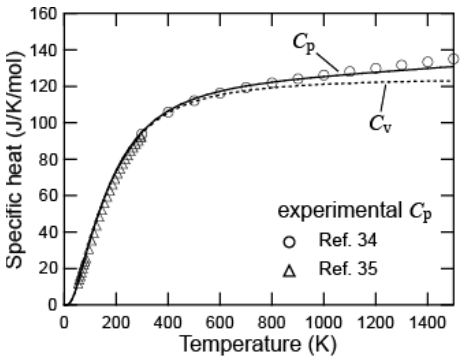

Figure 5. Molar specific heat at constant volume (C_v) and constant pressure (C_p) against temperature in β-Ga_2O_3.

Roy *et al* reported that an $\alpha \rightarrow \beta$ transformation occurs at 573 K under wet conditions and at 873 K under dry conditions, a $\varepsilon \rightarrow \beta$ transformation at 1143 K under dry atmosphere, and a $\delta \rightarrow \varepsilon$ transformation at >773 K under dry atmosphere [2]. Their back transformations have never been reported. The current results show that the β-phase is energetically most stable

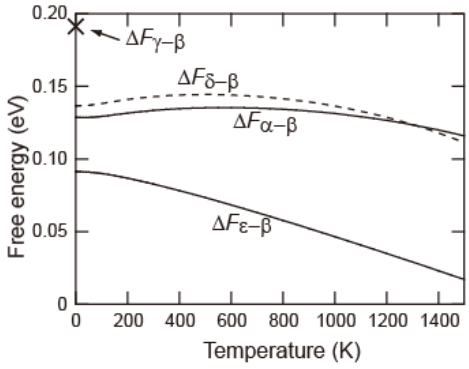

Figure 6. Temperature dependence of the differences in Helmholtz free energy per formula unit between α-, γ-, δ-, ε- and β-Ga_2O_3, $\Delta F_{\alpha-\beta}$, $\Delta F_{\gamma-\beta}$, $\Delta F_{\delta-\beta}$, $\Delta F_{\varepsilon-\beta}$, respectively.

and the ε-phase is more stable than the δ-phase at temperatures lower than 1600 K, which are consistent with these experimental observations.

4. Summary

The structures and energetics of five Ga_2O_3 polymorphs, α, β, γ, δ and ε, have been discussed using first-principles calculations. Taking κ-Al_2O_3 as a prototype, the geometry of ε-Ga_2O_3 with the space group $Pna2_1$ is optimized. The resultant lattice parameters are consistent with experimental results. The structure of γ-Ga_2O_3 is investigated assuming a defective spinel structure. 40-atom supercells with different atomic arrangements are employed, in which 2 Ga sites are chosen to be vacant among 18 sites. No clear preference for site occupancies is found among 14 inequivalent structures, which suggests a disordered distribution of vacancies at finite temperatures. Phonon dispersion curves of four polymorphs are computed with various lattice volumes. Within the QHA, volume expansivity, bulk modulus, specific heat at constant volume, and Helmholtz free energy are computed as a function of temperature. The expansivity increases in the order β, ε, α and δ, and the bulk modulus increases in the order β, ε, δ and α at low temperatures. The formation energies are in the order $\beta < \varepsilon < \alpha < \delta < \gamma$ at low temperatures. With the increase of temperature, the difference in free energy between the β-phase and the ε-phase becomes smaller, and vanishes at around 1600 K.

Acknowledgments

This work was supported by the 21st century COE program and Grant-in-Aids for Scientific Research (A) and Young Scientists (B) from the Ministry of Education, Culture, Sports, Science and Technology of Japan.

References

[1] Levin I and Brandon D 1998 *J. Am. Ceram. Soc.* **81** 1995
[2] Roy R, Hill V G and Osborn E F 1952 *J. Am. Chem. Soc.* **74** 719
[3] Orita M, Hiramatsu H, Ohta H, Hirano M and Hosono H 2002 *Thin Solid Films* **411** 134
[4] Matsuzaki K, Yanagi H, Kamiya T, Hiramatsu H, Nomura K, Hirano M and Hosono H 2006 *Appl. Phys. Lett.* **88** 092106
[5] Kroll P, Dronskowski R and Martin M 2005 *J. Mater. Chem.* **15** 3296

[6] Kroll P 2005 *Phys. Rev.* B **72** 144407
[7] Olliver B, Retoux R, Lacorre P, Massiot D and Ferey G 1997 *J. Mater. Chem.* **7** 1049
[8] Blöchl P E 1994 *Phys. Rev.* B **50** 17953
[9] Kresse G and Furthmüller J 1996 *Phys. Rev.* B **54** 11169
[10] Kresse G and Furthmüller J 1996 *J. Comput. Mater. Sci.* **6** 15
[11] Kohn W and Sham L J 1965 *Phys. Rev.* A **140** 1133
[12] Perdew J P, Burke K and Ernzerhof M 1996 *Phys. Rev. Lett.* **77** 3865
[13] Monkhorst H J and Pack J D 1976 *Phys. Rev.* B **13** 5188
[14] Kresse G, Furthmüller J and Hafner J 1995 *Europhys. Lett.* **32** 729
[15] Kunk K and Martin R M 1982 *Phys. Rev. Lett.* **48** 406
[16] Gonze X and Lee C 1997 *Phys. Rev.* B **55** 10355
[17] Baroni S, de Gironcoli S, Corso A D and Giannozzi P 2001 *Rev. Mod. Phys.* **73** 515
[18] Ahman J, Sevensson G and Albertsson J 1996 *Acta Crystallogr.* C **52** 1336
[19] Marezio M and Remeika J P 1967 *J. Chem. Phys.* **46** 1862
[20] He H, Blanco M A and Pandey R 2006 *Appl. Phys. Lett.* **88** 261904
[21] Goldschmidt V M, Barth T F W and Lunde G 1925 Geochemische Verteilungsgesetze der Elemente *Skr. Norske, Ved. Akad. Oslo Mat. K1* vol I–VIII
[22] Ueda N, Hosono H, Waseda R and Kawazoe H 1997 *Appl. Phys. Lett.* **70** 3561
[23] Tippins H H 1965 *Phys. Rev.* **140** A316
[24] Yamaguchi K 2004 *Solid State Commun.* **131** 739
[25] Reynolds D C, Look D C, Jogai B, Litton C W, Cantwell G and Harsch W C 1999 *Phys. Rev.* B **60** 2340
[26] Oba F, Nishitani S R, Isotani S, Adachi H and Tanaka I 2001 *J. Appl. Phys.* **90** 824
Oba F, Nishitani S R, Isotani S, Adachi H and Tanaka I 2001 *J. Appl. Phys.* **90** 3665
[27] Kresse G, Dulub O and Diebold U 2003 *Phys. Rev.* B **68** 245409
[28] Kohan A F, Ceder G, Morgan D and Van de Walle Chris G 2000 *Phys. Rev.* B **61** 15019
[29] He H, Orlando R, Blanco M A and Pandey R 2006 *Phys. Rev.* B **74** 195123
[30] Gutiérrez G, Taga A and Johansson B 2001 *Phys. Rev.* B **65** 12101
[31] Maradudin A A, Montroll E W, Weiss G H and Ipatva I P 1971 *Theory of Lattice Dynamics in the Harmonic Approximation* 2nd edn (New York: Academic)
[32] Poirier J P 2000 *Introduction to the Physics of the Earth's Interior* 2nd edn (Cambridge: Cambridge University Press)
[33] Eckert L J and Bradt R C 1973 *J. Am. Ceram. Soc.* **56** 229
[34] Mills K C 1972 *High Temp.-High Pressures* **4** 371
[35] King E G 1958 *J. Am. Chem. Soc.* **80** 1799